**Proceedings of ASME Turbo Expo 2011**
**GT2011**
**June 6-10, 2011, Vancouver, British Columbia, Canada**

**GT2011-45836**

# PROFILED ENDWALL DESIGN USING GENETIC ALGORITHMS WITH DIFFERENT OBJECTIVE FUNCTIONS

**Jamie McIntosh**
Now at: Royal Air Force
RAF College Cranwell
Sleaford, NG34 8HB
United Kingdom

**Richard MacPherson**
Now at: Airbus UK
New Filton House
Bristol, BS99 7AR
United Kingdom
richard.macpherson@airbus.com

**Grant Ingram*** **Simon Hogg**
School of Engineering
and Computing Sciences
Durham University
Durham, DH1 3LE
United Kingdom
g.l.ingram@durham.ac.uk
simon.hogg@durham.ac.uk

## ABSTRACT

*Profiled endwalls are a widely researched technology for reducing the secondary loss in turbines. Most designs in the literature have been produced directly by manufacturers and although general performance information is given the detailed design decisions are kept confidential. This paper outlines a simple design system for profiled endwalls that uses genetic algorithms to find an acceptable design. As the design process is produced in an academic environment full details of the design process, geometries produced, objective functions and the various trade-offs involved in the design are available and discussed in the paper.*

*Two designs were produced using the design system: one using secondary kinetic energy as the objective function of the design system and the second using a U-cubed integral. The different designs that are produced with the different objective functions are discussed in detail in the paper.*

*Finally profiled endwalls have traditionally been used in the high pressure stages of gas turbine blades, the paper also discusses the merits and challenges in applying these technologies to the high pressure and intermediate pressure stages of steam turbines.*

*Address all correspondence to this author.

## NOMENCLATURE

$a_o, a_n$ Fourier series coefficient
$A$ Area
$b_n$ Fourier series cosine coefficient
$C_{ax}$ Axial chord
$C_D$ Dissipation coefficient
$C_{p0}$ Total pressure loss coefficient $C_{p0} = \frac{P_{total_{ups}} - P_{total}}{\frac{1}{2}\rho V_{ups}^2}$
$C_{SKE}$ Secondary kinetic energy coefficient $C_{SKE} = \frac{U_{sec}^2 + U_r^2}{U_{ups}^2}$
$f_{C_{SKE}}$ Secondary kinetic energy coefficient cost function
$f_{cost}$ Cost function
$f_{U^3}$ Velocity cubed cost function
$f_{yaw}$ Yaw cost function
$L$ Curve length
$\dot{m}$ Mass flow
$Ma$ Mach number
$n$ Number of cycles
$P_{total}$ Total pressure
RCL Reverse compound lean
RNG Re-Normalisation Group
$Re$ Reynolds number based on exit velocity and axial chord
$S$ Entropy
$\dot{S}_a$ Entropy production per unit area
$t$ Tangential coordinate
$t$ Temperature

$U$ Velocity
$U_r$ Radial velocity
$U_{sec}$ Secondary velocity
$U_{ups}$ Upstream velocity
$W_{C_{SKE}}$ Weight component of secondary kinetic energy coefficient
$W_{yaw}$ Weight component of yaw angle
$\alpha$ Yaw angle
$\alpha_{chrom}$ Yaw angle for individual chromosome
$\alpha_{mid}$ Midspan yaw angle
$\alpha_{planar}$ Yaw angle for the reference case
$\beta$ Pitch angle
$\delta$ Boundary layer thickness
$\tau$ Shear stress
$\rho$ Density

## INTRODUCTION

Secondary flows are a major source of loss across turbomachinery blades. One of the most successful recent methods for attacking this loss has been non-axisymmetric endwall profiling see for example: Harvey et al. [1,2] or Praisner et al [3]. Endwall profiling is the process of contouring the hub of the turbomachine around the base of the blade to redirect the flow to reduce secondary losses and improve the efficiency.

Previous designs produced have largely been generated by engine manufacturers and the publication of the results has been constrained by both commercial and industrial concerns. This paper outlines a simple but open design system for which both the code and the geometries that are produced are available for detailed inspection. An open access design system allows the endwall geometry to be recreated potentially allowing researchers to collaborate.

This paper first outlines the design system used at Durham, then describes two designs produced for the Durham Cascade a geometry known for complex secondary flows. Finally the implications of adding profiled endwalls to steam turbines stages are discussed.

## BACKGROUND

Secondary flows in turbomachines are produced by the non-uniform flow at inlet to a blade row, usually due to the end wall boundary layers, but also from other non-uniformities in total pressure or temperature. In turbines their importance is significant as a source of loss, which may be a large proportion of the total loss, particularly in low aspect ratio blades, such as in a high-pressure gas or steam turbine. Thus secondary flows have been studied for many years.

Sieverding [4] and Langston [5] describe in detail secondary flows. The actual form of this secondary flow is highly complex

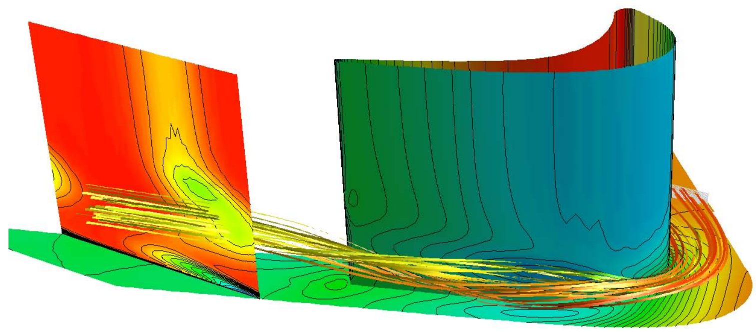

**FIGURE 1**. SECONDARY FLOW FEATURES

but there are three principle features: The Passage Vortex, The Horseshoe Vortex and the Corner Vortex.

The Passage Vortex is the dominant feature of secondary flow within the blade passage and can be seen in numerous experimental results [6], [7] and [8]. The passage vortex is formed across the blade passage, the cross passage pressure gradient (from the suction surface of the blade to the pressure surface) affects both the boundary layer fluid and the mid-span flow. The boundary layer velocities are slower relative to the mid-span flow, and therefore follow a tighter radius of curvature. A tangential flow across the passage is created and to preserve continuity, a vortex is formed.

The Horseshoe Vortex is formed at the leading edge of a blade and is produced when the inlet boundary layer meets the blunt leading edge of the blade. The mainstream flow has a higher stagnation pressure than that of the flow nearer the endwall and hence a radial pressure gradient is formed on the blade leading edge. This results in the formation of a vortex structure which moves tangentially around both sides of the leading edge. Eckerle and Langston describe this feature in great detail [9].

The Corner Vortex, or sometimes know as the Counter Vortex, is caused by the cross flow underneath the passage vortex interacting the blade suction surface in a similar manner to the horseshoe vortex. The feature is relatively small compared to the other vortical structures and is only present in experiments with high turning flows.

An illustration of the complexity of the secondary flows encountered in turbines is found in Figure 1 which shows a visualisation of one of the calculations shown in this paper. The streamlines highlight the passage vortex, whilst the blade surface shows contours of static pressure, a plane through the flow at the exit of the domain shows total pressure highlighting the high loss regions associated with the blade wake and the passage vortex.

With the drive for higher stage loading and increased efficiency interest in reducing secondary flows has continued, and some of the methods used are reviewed by Praisner et al [3]. The methods may be grouped into three categories:

Firstly, there are methods which rely on modifying the end wall profile. This was first done axisymmetrically (circumferentially uniform) such as described by Atkins [10], but the results tended to show a redistribution of loss rather than a reduction. Much more success has been achieved with non-axisymmetric profiling, where an endwall shape with no symmetry is used. Although the idea of non-axisymmetric profiled end walls is quite old, most of the current work takes its foundation from the work of Rose [11] who designed end walls to control the static pressure distribution at exit from a blade row. The idea was extended to control secondary flow and many papers have been published on its application and introduction in real machines, such as Harvey et al [1], Hartland et al [2], Brennan et al [12] and Harvey et al [13]. The principle of endwall profiling is that of introducing streamline curvature into the blade passage, where concave curvature would be used to increases the local static pressure, and hence reduce the local velocity. Convex curvature would reduce the static pressures and increase the fluids local velocity. By appropriate profiling the cross passage pressure gradient can be reduced and secondary flows minimised.

Secondly there are methods which alter the blade stacking, usually in the tangential direction. This was investigated by Harrison [14] among others, who investigated straight lean and positive compound lean, where the suction surface makes an obtuse angle with the end wall at both ends of the blade. This showed improved radial uniformity of exit flows but no overall loss reduction. Sharma et al. [15] also investigated blade lean, and showed a reduction in loss with reversed compound lean (RCL) where the suction surface makes an acute angle with the end wall at both ends of the blade. Bagshaw et al [16] also investigated the effects of RCL and showed increased intensity of secondary flows, but reduced profile loss in the mid section, giving an overall reduction in loss.

Thirdly there are methods which alter the blade profile near the end wall. Some early results were presented by Sauer [17] using bulbs on the leading edge. They showed significant reductions in secondary flows attributed to affecting the horseshoe vortex. There have been further studies with different shapes near the end wall, such as Saha et al [18]. There are also studies with fillets on the blade to end wall junction, such as Zess and Thole [19] and Becz et al [20].

Finally a number of authors have combined these different features to develop "shaped passages" rather than distinct endwalls, blades and features. The first example of this is the work of Nagel and Baier [21] who generated a loss minimising geometry based on an LP turbine profile, T106, using both aerofoil and end wall modifications in an automated optimisation process. Another example is that of Bagshaw et al. [22], [23].

The Durham Cascade is a physical model of the Rolls-Royce RB211 high pressure turbine which allows researchers to understand the complex flow patterns, whilst removing the annular features of the geometry and moving parts found in a real machine. The flow still remains complex and the work of Haller and Anderton [24] illustrates that the key flow features in real machines are also found within cascades. Cascade testing is therefore a good place to do wide ranging speculative investigations of future technologies. Table 1 shows the key features of the Durham Cascade with 110° of turning the cascade features strong secondary flows.

**TABLE 1**. DURHAM CASCADE PARAMETERS

| | |
|---|---|
| Inlet Flow Angle | $42.75^o$ |
| Turbulence Intensity | 5% |
| Blade Exit Angle | $-68.7^o$ |
| Blade Axial Chord | 181mm |
| $Re$ | $4.0 \times 10^5$ |
| $Ma$ | 0.1 |

## RATIONALE FOR THE ENDWALL PROFILE DESIGN SYSTEM

The details of the design system used at Durham are described by MacPherson [25], [26] and the latest developments by McIntosh [27]. An outline of its rationale is provided here.

Optimisation techniques can be divided into two types; gradient and non gradient methods. Gradient methods linearise, using a Taylor series expansion, both the objective function and constraints and from these first order sensitivities are calculated. These sensitivities express how the objective responds to specific design changes. A well know drawback of gradient methods is that the method does not take into account noise and discontinuities that might exist within the design space.

Non Gradient methods use randomised probabilistic searches to find the optimum solution, these are commonly known as heuristic methods which are able to locate feasible solutions that are reasonably close to being optimum for the problem. Genetic algorithms are seen as an attractive heuristic method due to their ease of use and robustness as documented in Goldberg [28]. They allow optimisation of a multi-objective design space and reach an acceptable solution even when the objective function is noisy.

Genetic Algorithms are a novel solution in optimising endwall profiles, allowing the effects of introducing variable geometry into the domain to be clearly understood. The disadvantage is the large computational cost that they incur, for this application the authors chose to sacrifice computational time in pursuit a more general method.

## CFD VALIDATION

Before any optimisation took place the CFD model was validated by comparing computations to experimental data. This is

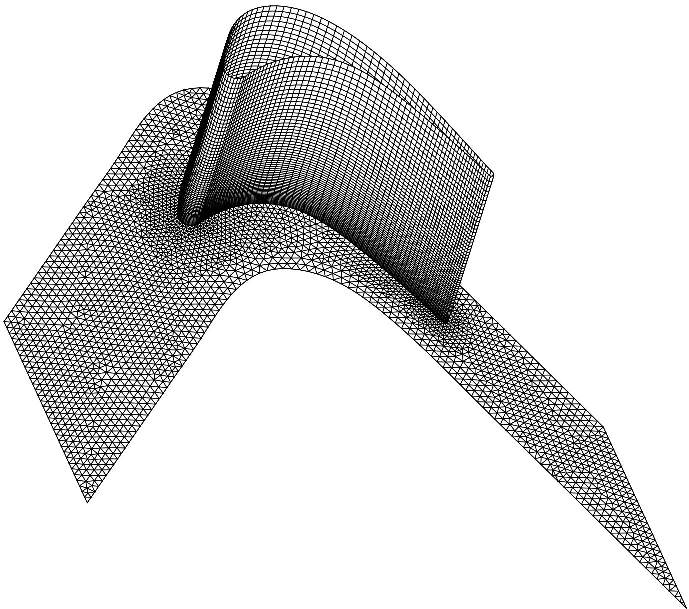

**FIGURE 2**. PLANAR ENDWALL MESH

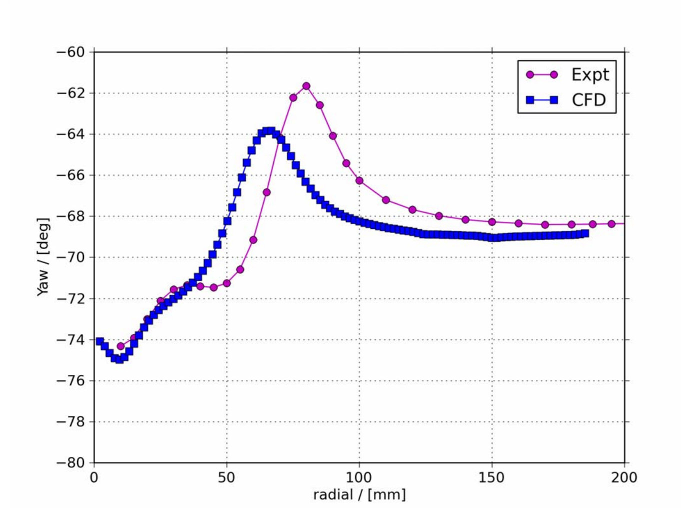


**FIGURE 3**. EXPT. AND CFD PITCH AVERAGED YAW ANGLE

vital for accurate work as Ingram et al. [29] showed even validated CFD solutions can produce misleading results.

Throughout this work CFD results were compared to experiments conducted at 128% axial chord, or 51mm downstream of the blade's trailing edge.

A geometry and mesh generation package known as *Gambit* was used to parametrise the blade passage. Mean-line blade vertex data was imported and offset by $\pm\frac{191}{2}$mm in the tangential direction to create a two dimensional blade passage. This domain was extended 100% $C_{ax}$ upstream of the leading edge and 78% $C_{ax}$ downstream of the trailing edge. An unstructured mesh was used for the primary reason that it was simpler to set up. To capture the effects of the boundary layer the mesh in the radial direction was refined. As the flow pattern was symmetrical about the mid-span of the blade, only half the span was modelled.

To ensure the flow field and secondary effects were accurately captured, a convergence analysis was performed. A range of mesh densities were chosen from approximately 18,000 to 600,000 elements and CFD analysis was conducted on each mesh design after refinement. For each case, the area averaged yaw angle was calculated. After approximately 300,000 elements, the accuracy of the solution stabilised. From this, it was decided that approximately 300,000 elements would be used to model the flow field.

Figure 2 shows the final mesh along with the span-wise refinement on the blade surface and local refinement at the blade's leading and trailing edges. For the Planar Endwall Model, all elements had an aspect ratio less than 100 and the average skewness value below 0.6 indicating a good quality mesh. Both quality parameters are used throughout the design system.

Throughout this work, the Re-Normalisation Group (RNG) $k-\varepsilon$ model was used, which re-normalises the Navier-Stokes equations, to account for the effects of smaller scales of motion that exist within the flow structure. A variety of model constants were examined, however it was found that the default constants set in *Fluent* provided an accurate enough solution. The boundary condition at inlet was set as a velocity profile taken from previous measurements in the cascade. The turbulence conditions at inlet were set with a turbulence intensity of 5% and length scale of 0.936mm as specified in Gregory-Smith and Moore [30]. The exist was set as a pressure outlet and the midspan was set as a symmetry plane.

Second order upwind schemes were used to achieve discretisation of the governing equations and the pressure-based coupled solver from *Fluent* was used. This produced considerable benefits over the *SIMPLER* pressure-velocity coupling scheme used previously. The under relaxation values were left at default values, from which the analysis was initialised. Computation was performed on the Durham University high speed computing service known as Hamilton. The model was submitted to the cluster, iterated and acceptable convergence was achieved when the residuals of all three velocity components and momentum dropped below $10^{-4}$.

The yaw angle predictions compared to some experimental results are shown in Fig. 3, illustrating that the flow structure is well captured although the loss predictions (not shown) are worse. Overall the numerical results are as good or better than those used by Harvey et. al. [1] and were deemed reliable enough to base an optimisation method upon.

## ENDWALL PARAMETRISATION

A Fourier series (Equation 1) was used to parametrise the endwall in the same manner as Harvey et al [1]. The series constants $a_0$, $a_n$ and $b_n$ determine the amplitude and phase of each harmonic and can be summed linearly to determine the characteristic shape of the series.

$$f(t) = a_0 + \sum_{n=1}^{\infty} \left( a_n \cos \frac{n\pi t}{L} + b_n \sin \frac{n\pi t}{L} \right) \tag{1}$$

Using Fourier series curves ensured that the cross sectional area of the endwall remained constant. This method of parametrising the endwall surface was used in this paper.

The first harmonic of the Fourier series were used, with the first constant $a_0$ always being zero so any positive perturbation is cancelled out by a negative perturbation, the aim being to keep the passage area constant throughout. This is important as it is very easy to decrease loss by simply reducing the mass flow through and hence the loading of the blade row.

Originally two harmonics were used in the production of designs [26] but the resultant designs were geometrically very complex. An objective of this work is to understand the relationship between the design system and the resultant geometry so a single harmonic was chosen for this study.

To form the endwall surface, six Fourier series curves were imported into the domain at different axial locations. Through each curve, non uniform rational B-splines were plotted whose start and end values are found on the existing edges of the planar computational model. A net surface was then generated which produced a 3D contoured surface over the Fourier series curves and the boundary conditions from the planar model were used.

To streamline the process of meshing the domain and running the flow analysis, journal scripts were developed in both *Gambit* and *Fluent* to automate the procedure. Developing these processes is a non-trivial task. After some effort a reliable method for meshing non-axisymmetric endwalls was developed.

## ENDWALL PROFILE DESIGN SYSTEM

There are seven main stages in the design system: *i*) Initialising the algorithm & generating the initial population; *ii*) Generation & computation of each chromosomes CFD model; *iii*) Analysing the cost function of each chromosome; *iv*) Selecting, mating, mutation and generation of new population; *v*) Generation & computation of each chromosome CFD model; *vi*) Analysing the cost function of each chromosome; and finally *vii*) Convergence check

The software was developed using the *Octave* programming language. The main core of the genetic algorithm has been adapted from Haupt & Haupt [31]. However, extensive development of the code was required to interface the CFD analysis and data processing software into the algorithm.

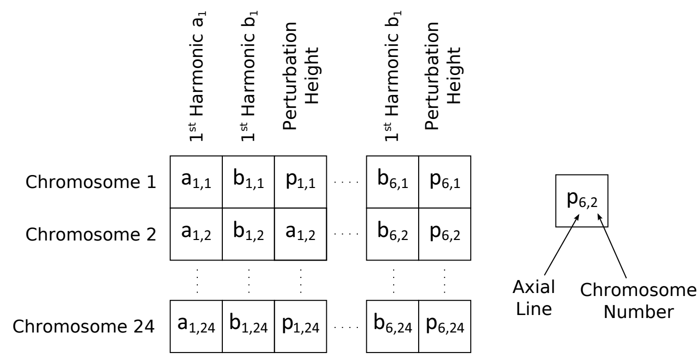


**FIGURE 4**. FORMAT OF GEOMETRY MATRIX

The initial geometry matrix contained all the data necessary to create a set of six axial curves for each chromosomes of a generation. Each chromosome was defined as an array of $1 \times 18$ elements with blocks of 3 elements containing the data for a single line. The first two terms generated the shape of the Fourier series curve and the third determined the maximum perturbation height. Since there were 24 chromosomes in each population a $24 \times 18$ matrix was produced for each generation. The format is illustrated in Figure 4.

For all design studies in this report, the maximum radial perturbation height was restricted to $\pm 20mm$ as this could be easily manufactured.

Once the Genetic Algorithm had been initialised, an initial chromosome population was generated by populating the variable matrix with random numbers, each of which were normalised by the design constraints.

The design variables for each chromosome then generated six comma separated files containing Fourier series curve vertex data at each of the six axial locations. These files were then submitted to the cluster along with mesh and flow analysis journal files. Once the geometry had been parametrised and the mesh generated in *Gambit*, CFD flow analysis was performed on each chromosome in *Fluent*. To reduce CFD processing time the planar case was used to determine the initial conditions for the CFD flow analysis.

Once the CFD was complete two ASCII files were generated $100\%C_{ax}$ upstream of the leading edge and $28\%C_{ax}$ downstream of the trailing edge. These results files were then processed to give pitch and area averaged data. The key variables were extracted to determine the cost of the chromosome. This process was repeated for each chromosome.

After the cost of all chromosomes had been determined, the fitness of each chromosome was evaluated to determine whether it was fit enough to survive and possibly reproduce offspring to generate the next generation. To achieve this, the chromosomes were ranked from lowest cost to highest cost. Of the eight chromosomes, the top four were kept for mating and the remainder discarded. This process mimicked natural selection, with only the fittest chromosomes being taken forward to generate the next population.

The top four chromosomes formed the mating pool from which mother and father pair randomly. Each pair produced two offspring that contained traits from each of the parents creating four new chromosomes. The process of mating used an extrapolation method with crossover developed by Michalewicz [32]. A variable in the chromosome was randomly selected as the crossover point, from which the selected variables were combined to form new variables that appear in the offspring generated. In addition, both pairs of parents survived, creating the next population of eight chromosomes.

To avoid the genetic algorithm converging too quickly, which could occur if the solution settles in a local minimum rather than the global optimum, mutation was introduced into the design system. This forced the algorithm to explore other areas of the cost surface by randomly introducing changes, or mutations, to some of the variables. The mutation rate was set at 20% and randomly selected locations within the matrix were selected and replaced with a uniform random number.

After selection, mating and mutation, the next generation was formed and the process of generating the Fourier series curves, submitting the chromosomes to Hamilton and calculating the cost function from data processed information was iterated until acceptable convergence was achieved.

The aim of the Genetic Algorithm was to find the global minimum of the cost function. After the cost of each generation had been calculated, the algorithm checked whether the solution had converged against previously specified criteria. If this had not been achieved, the process of iterating the solution would continue until acceptable convergence has been achieved or when the maximum number of iterations had been exceeded.

The Genetic Algorithm analysed 100 generations containing 24 chromosomes for two different cases that, in total, required the computation of 4801 CFD runs including the planar case. Each run would have taken about forty minutes of clock time to run on the cluster but including local processing time, the algorithm had the potential to complete within 4 days. However, due to high cluster load the authors were only able to compute each design solution over the course of a week.

If the geometry failed to mesh or the flow analysis did not convergence, the cost function was set to 1000, which ensured that upon selection, these chromosomes were killed and their contributions would not propagate any further into the analysis. This would occur if the endwall profile involved sharp sudden changes in geometry preventing mesh elements being mapped onto the face. If meshing of this geometry was successful, elements were often of poor quality and contained a high degree of equiangle skew causing the CFD flow analysis to fail.

It is undesirable to have sudden changes in the endwall profile, as this may result in adverse flow effects being generated. If the chromosome is not allowed to mate, these sudden changes in geometry are not allowed to propagate through the solution, resulting in smoother endwall profiles being generated. The scheme also allows the genetic algorithm to explore all potential solutions on the cost surface. If CFD analysis cannot be performed on the chromosome, the genetic algorithm continues to search for the final optimal solution without the need for the user to intervene. This adds a degree of artificial intelligence to the algorithm, ensuring sharp geometry is not allowed to propagate through the analysis. In practise the percentage of "killed" chromosomes was very low with only a handful of the runs failing.

The algorithm was initialised as a minimisation problem, whose aim was to reduce the objective function. One hundred generations were run to obtain the final result.

## COST FUNCTIONS

Two different cost functions were used in preparing the designs produced in this paper. The first, secondary kinetic energy coefficient $C_{SKE}$ indicates the amount of secondary kinetic energy that is present in the flow at each radial position. The second is based on a integral of the cube of the surface velocity. The cost function is the key mechanism used to avoid the production of incorrect designs, it is vital that the optimser is provided with a cost function that the CFD can predict.

The secondary kinetic energy coefficient is defined as:

$$C_{SKE} = \frac{U_{sec}^2 + U_r^2}{U_{ups}^2} \tag{2}$$

where $U_{sec}$ and $U_r$ are given by:

$$U_{sec} = U \sin(\alpha - \alpha_{mid}) \tag{3}$$

$$U_r = U \sin\beta \tag{4}$$

This definition of secondary kinetic energy is straightforward as the subject of this paper is a linear cascade with prismatic blades and a clearly defined mid-span flow. In real turbomachines more complex definitions often using helicity are used [12].

In a theoretical ideal case, no secondary kinetic energy would be present in the flow and hence $C_{SKE}$ would be zero throughout the domain. As the flow passes through the blade passage, the fluid is turned by the blade and the magnitude of this turning is indicated in the area averaged yaw angle. Ideally this would remain at the mid-span yaw angle of $-68.7^o$ degrees up the span of the blade.

The cost function (Equation 5) included a logic statement such that if the flow was overturned $f_{yaw}$ was set to zero.

$$
\begin{aligned}
f_{cost} &= f_{C_{SKE}} + f_{yaw} &(5)\\
&= \left[(100 \times C_{SKE}) \times W_{C_{SKE}}\right] &(6)\\
&+ \left[\left(\alpha_{planar} - \alpha_{chrom}\right) \times W_{yaw}\right] &(7)
\end{aligned}
$$

$C_{SKE}$ was magnified by a factor of 100 to ensure that both parameters were of the same order of magnitude. The weights for each component were $W_{C_{SKE}} = 0.7$ and $W_{yaw} = 1$.

Denton [33] reasons that the only rational measure of loss is entropy creation. This is because the flow in most machines is closely adiabatic and so only entropy creation due to irreversibilities contributes significantly to the loss of efficiency.

$$\dot{S}_a = \int_0^{\delta} \frac{1}{T}\, \tau \, dU \tag{8}$$

Equation 8 is used to determine the entropy generation per unit surface area within a boundary layer and can be thought of as viscous shear work being converted irreversibly to heat. Most importantly it shows that entropy generation is proportional to velocity and shear stress. Velocity changes most rapidly near the surface and so most of the generation can be considered to be concentrated within the inner part of the boundary layer.

It is often more convenient to refer to the entropy production rate from a dimensionless dissipation coefficient as given by Equation 8:

$$C_D = \frac{T \dot{S}_a}{\rho U_\delta^3} \tag{9}$$

With simple rearrangement it can be shown that:

$$\dot{S}_a = \frac{\rho C_D}{T} U_\delta^3 \tag{10}$$

Since dissipation varies as the cube of velocity the entropy generation rate is proportional to the cube of velocity. The velocity represented in Equations 9 and 10 is the velocity at the edge of the boundary layer and if the integral of this velocity is taken across the entire surface of the blade passage then a valuable measure of the total entropy on the surfaces can be determined.

Using the relationship in Equation 10, where the entropy generation rate is proportional to the surface integral of the cube of velocity, it was possible to determine a measure of loss within the system.

$$\dot{S}_a \propto \int_0^{\delta} U^3 \, dA \tag{11}$$

The isentropic, or non-slip velocity was used in this calculation because the velocity at a surface is always zero. To calculate the flow velocity at the surface the relationship in Equation 12 was used.

$$U = \sqrt{\frac{2(P_{total} - P)}{\rho}} \tag{12}$$

A surface integral report for $U^3$ over the surface of the blade and endwall was generated using *Fluent*. This ASCII file was processed using the local data post-processor, *importfile*, to evaluate designs that examined $\int U^3 dA$ as part of its cost function.

The cost function in the optimisation included the yaw angle component as for the $C_{SKE}$ cost function:

$$
\begin{aligned}
f_{cost} &= f_{U^3} + f_{yaw} &(13)\\
&= \left[\left(100 \times \int U^3 dA\right) \times W_{U^3}\right] &(14)\\
&+ \left[\left(yaw_{planar} - yaw_{chrom}\right) \times W_{yaw}\right] &(15)
\end{aligned}
$$

The weights for each component where $W_{U^3} = 1$ and $W_{yaw} = 1$ as preliminary calculations showed they had the same order of magnitude.

## Profile Endwall Designs

The final endwall geometries produced by each complete run of the design system are shown in the 2D contour plots of height Fig. 5 for the $C_{SKE}$ design and Fig. 6 for the $U^3$ design. The scale is in mm above and below the planar case.

## The $C_{SKE}$ Design

Figure 5 was the best design produced from 100 generations that minimised $C_{SKE}$ and penalised flow under turning. Overall

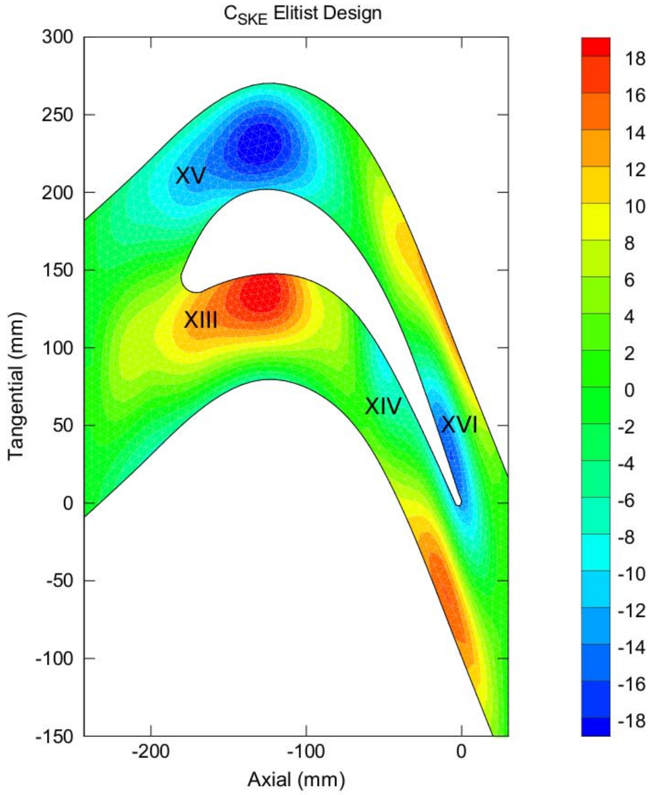


**FIGURE 5**. $C_{SKE}$ Design (Contours in mm)

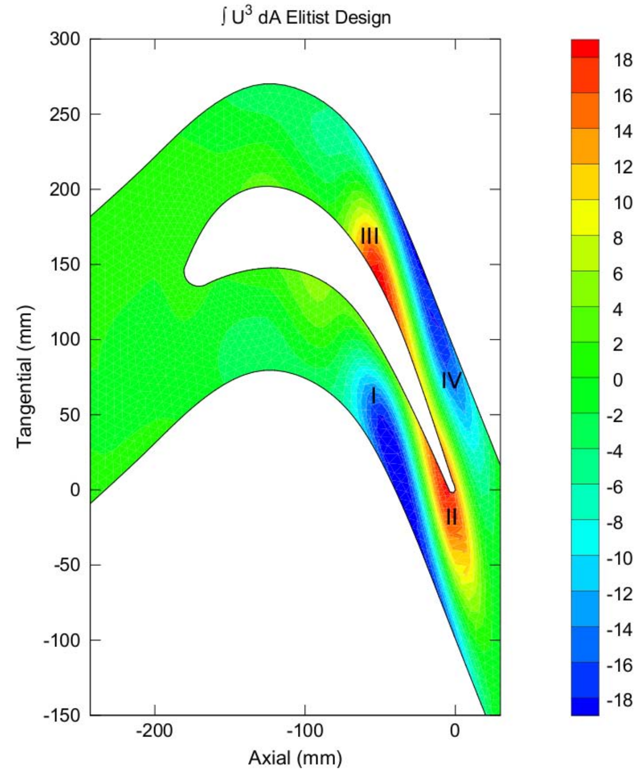


**FIGURE 6**. $U^3$ Design (Contours in mm)

the geometry produced by this design is similar to other designs using a similar methodology [34] with the pronounced hump (XIII) and dip (XV) upstream following the logic of a reduced cross passage pressure gradient. At the trailing edge a further hump and dip combination is put in place, a geometrical feature which slows the development of the counter or corner vortex.

Examining the pitch averaged data (Figs. 10 and 11) reveals the amount of under turning has been reduced by approximately 5° and the amount of overturning near the endwall has increased by 3°. The point of maximum under turning has moved closer to the endwall surface indicating a reduction in strength of the passage vortex. The loss coefficient shows a shift of loss core towards the endwall consistent with Fig. 8.

The total pressure loss coefficient for the $c_{SKE}$ design (Fig. 8) is compared with the planar case in Fig. 7. A single loss core is confirmed (A) that has increased in size due to the combined merging of the passage vortex with the horseshoe vortex. The reduced secondary velocity magnitude of the vortex structures suggests that the combined loss core is most likely the result of a CFD simulation which over emphasises the influence of viscosity. The increased strength of the corner vortex (D) can also be seen as acting over a larger tangential region.

Area averaged results of all major parameters including $C_{SKE}$ are presented in Table 2. The $C_{SKE}$ endwall design showed a significant reduction in the passage vortex and resultant secondary flows causing a total $C_{SKE}$ reduction of 67.7%. This reduction is the most ever obtained by a profiled endwall design for the Durham Cascade with examples from [35], [1] and [25] achieving reductions of 55%, 40% and 29% respectively in their CFD calculations. Table 2 shows a modest increase in loss but previous work [29] has shown that RANS estimates of loss for profiled endwall design do not correlate well with reality and the values are included largely as a reference.

## The $U^3$ Design

Figure 6 was the best design produced from 100 generations that minimised $\int U^3 dA$ and penalised flow under turning. This is the first reported use of the $U^3$ integral method to parametrise an endwall surface to reduce losses within a blade row.

On the suction surface, the flow is accelerated from 30% $C_{ax}$ upstream of the trailing edge (III) where it then enters a high local pressure field (IV) before interacting with the positive perturbation at the trailing edge (II).

As can be seen in the pitch averaged plots, Figs. 10 and 11 this design has increased the amount of under turning by approximately 1.5° and overturning near the endwall surface by 5°. The

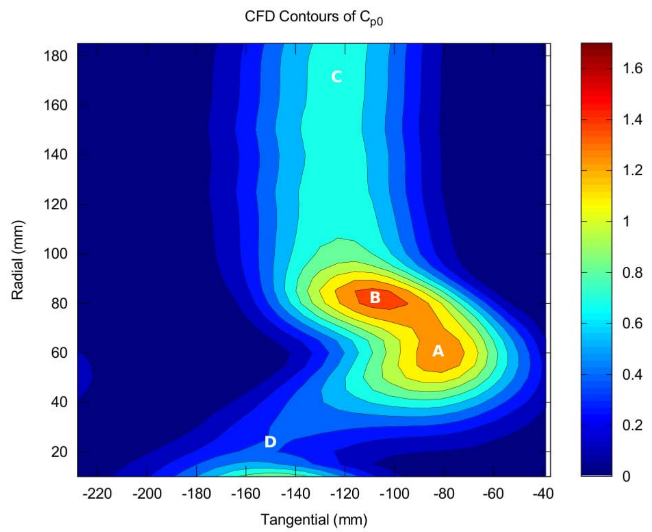


**FIGURE 7**. LOSS CONTOURS FOR THE REFERENCE

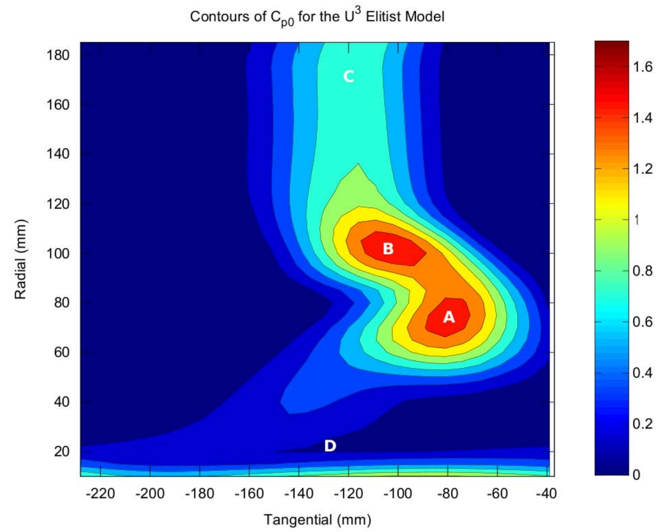


**FIGURE 9**. LOSS CONTOURS FOR $U^3$ DESIGN

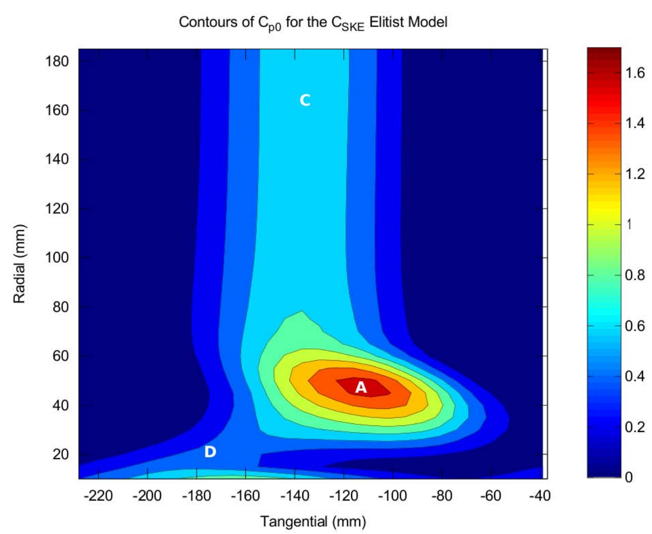


**FIGURE 8**. LOSS CONTOURS FOR $C_{SKE}$ DESIGN

**TABLE 2**. AREA AVERAGED RESULTS

| | Planar | $U^3$ | $C_{SKE}$ |
|---|---|---|---|
| Area Avg. $C_{SKE}$ | 0.0569 | 0.0668 | 0.0184 |
| Percentage $C_{SKE}$ | 100% | 117.4% | 32.3% |
| Area Avg. $\int U^3 dA$ | 4341.89 | 3692.76 | 4813.98 |
| Percentage $\int U^3 dA$ | 100% | 85.0% | 110.9% |
| Area Avg. $C_{P0}$ | 0.3085 | 0.3179 | 0.3270 |
| Percentage $C_{P0}$ | 100% | 103.0% | 105.9% |
| $\dot{m}/[kg/s]$ | 0.571 | 0.571 | 0.573 |
| Mass avg. $\alpha/[°]$ | -69.1 | -69.1 | -70.7 |

radial shift of the point of maximum under turning away from the endwall surface is associated with an increase in strength of the passage vortex. The most striking part of Fig. 10 is that the midspan yaw angles do not converge on the same value. These changes have been attributed to two factors, firstly the simulation has a prescribed velocity at inlet so as the secondary flows are reduced for the $C_{SKE}$ case the mass flow through the cascade rises somewhat (Table 2). Secondly for the $\int U^3 dA$ design the extent of the secondary flows has actually increased, secondary flows activity precedes loss and so Fig. 9 under-reports this activity and the actual influence of the enhanced secondary flow extends quite close to midspan where a symmetry boundary condition may no longer be appropriate in the simulation.

The total pressure loss coefficient of the $\int U^3 dA$ design (Fig. 9) is compared to the planar case in Fig. 7. The loss cores of the passage (A) and suction side horseshoe (B) vortices are located further away from the endwall and their magnitudes show a slight increase as supported by the pitch averaged data. The width of the blade wake (C) remains constant. The corner vortex (D) can be seen to have increased to cover the full tangential plane.

Figure 9 shows the increased interaction between the passage vortex (A) and the corner vortex (D). Secondary flows within the corner vortex have increased causing a reduction in secondary flow near the endwall surface. This in turn reduces the sum of the $U^3$ integral. The horseshoe vortex (B) and the

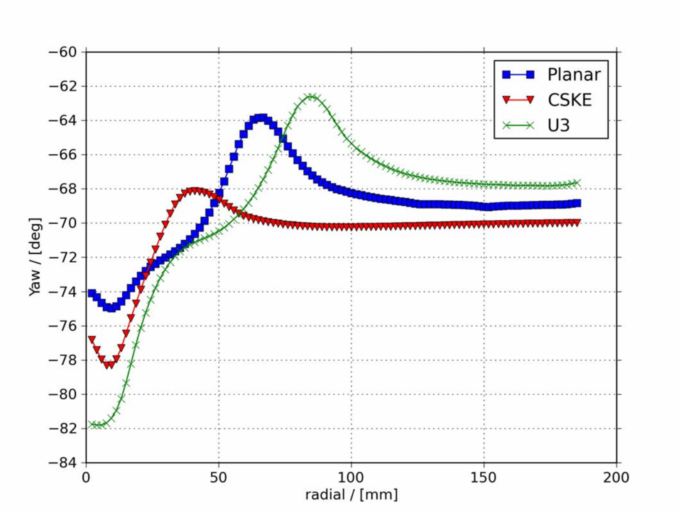


**FIGURE 10**. PITCH AVERAGED YAW ANGLE

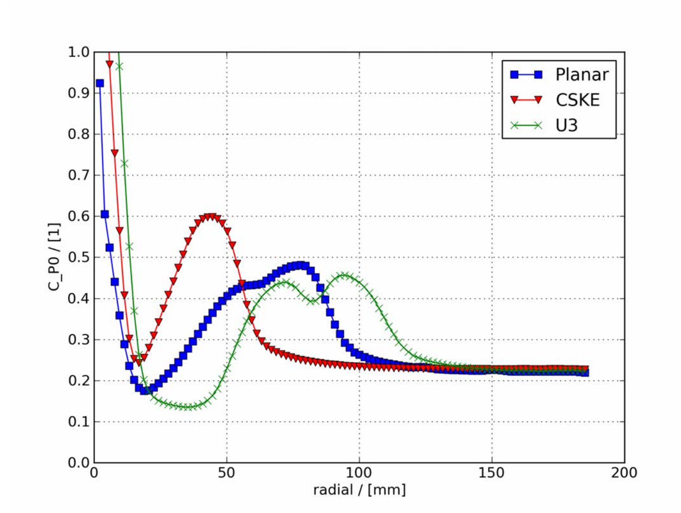


**FIGURE 11**. PITCH AVERAGED LOSS COEFFICIENT

passage vortex (A) remain distinct.

The change in $\int U^3 dA$ for the candidate designs is provided in Table 2. The $U^3$ endwall reduces this parameter by 15.0% suggesting a loss in entropy generation within the blade and endwall boundary layers. The corner vortex is enhanced over the full tangential plane increasing the interaction with the passage vortex. The counter-rotating nature of the corner vortex takes secondary kinetic energy out of the passage vortex near to the endwall reducing the flow velocity at the endwall surface. The problem with the $U^3$ integral method is that it only minimises losses at surfaces and so neglects to consider the passage vortex which is a major source of loss. As a single criterion, therefore, the $U^3$ method is unsuitable for use in profiled endwall design.

Table 2 shows that the $C_{SKE}$ design reports an increase in $\int U^3 dA$ of 10.9% and the $U^3$ design exhibits a modest increase in the calculated value of loss coefficient. The optimisation system has been successful in keeping the mass weighted yaw angle at or above the target value for both designs.

In order to further understand the behaviour of the $\int U^3 dA$ design streamlines in the CFD result were plotted. This shows that convex curvature at the trailing edge for the $U^3$ design forms an acute corner which encourages the formation of the corner vortex as shown in Fig. 12. The corner vortex interacts with the passage vortex to create a flow region near the endwall with low secondary kinetic energy. The other vortex structures appear to remain unaffected confirming that the $U^3$ method is only able to minimise surface loss.

The $U^3$ design enhances the presence of the corner vortex whilst the passage vortex is displaced radially causing $C_{SKE}$ to increase by 17.4%. Experimentation on this design would reveal the extent of loss reduction as a result of optimising the $U^3$ integral as currently it is unclear whether there is an overall benefit gained by the system.

## DISCUSSION

The $U^3$ integral method sums the total contribution from the endwall and blade surfaces. The design system has no influence on the blade surface and so the combined sum possibility limits the outcome of design. The design produced was successful at reducing the $U^3$ integral but it would be of interest to use the design system to produce a design that only considered contributions from the endwall to observe effects.

It has been observed that modifying the cost function produced different endwall designs. The $U^3$ cost variable in this report is limited because of its inability to modify the shape of the blade. Haller and Anderton [24] were successful at reducing the $U^3$ integral on a blade surface because of the largely 2D blade losses that could be reduced. They achieved this by specifying geometric relationships for the blade shape that could be modified by a design system. The $U^3$ method used in this report is unsuitable to produce profiled endwall designs because it is unable to account for 3D losses within the blade passage.

## APPLICATION TO STEAM TURBINES

Turbine blade passages featuring profiled endwall designs have now entered service successfully and are becoming a standard feature of the latest generation of gas turbine designs [12]. The same cannot be said for steam turbines. The short height blades on steam turbine high pressure and intermediate pressure cylinders have aspect ratios and loadings similar to those of gas turbine stages. The potential exists to exploit similar performance benefits to that achieved on gas turbines, by applying profiled endwalls on these steam turbine stages.

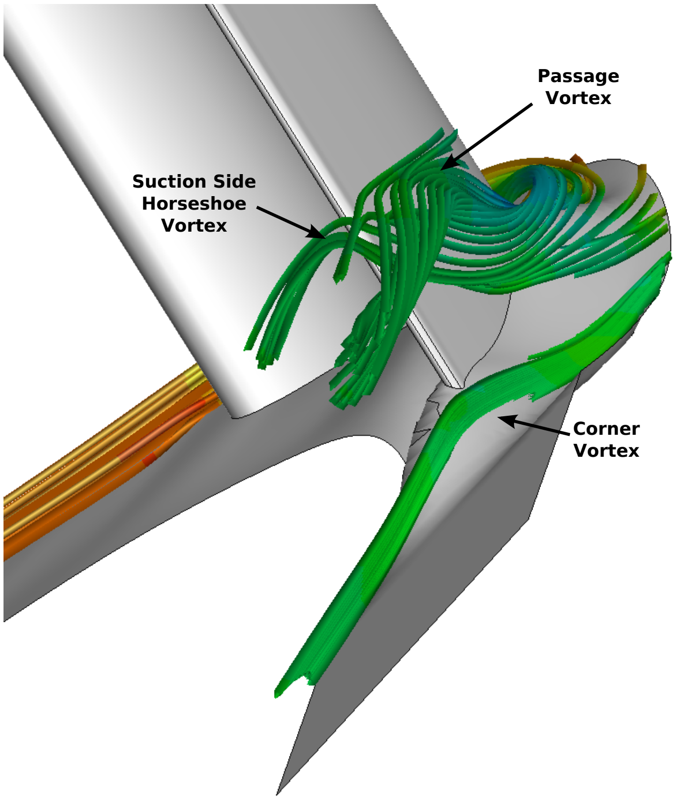


**FIGURE 12**. Visualisation of Flow Features within the $U^3$ Endwall

The current state-of-the-art in the development of modern 3-D steam turbine blade design is to control secondary flows and reduce losses through the 3-D stacking for the blade aerofoil. ALSTOMs controlled flow nozzle technology [36] is one such example. In this concept, the aerofoil is rotated about the blade trailing edge so that the throat area is opened up at mid-span and closed down approaching the blade endwalls. This has the effect of pushing more of the flow through the mid-span on the blade away from the endwall regions, thereby weakening the secondary flow features in the flow through the nozzle. The re-distribution of flow required to achieve this is controlled in such a way that any negative impact on the performance of the subsequent moving blade is minimised, so overall stage efficiency is increased.

Historically, sealing has received the most attention in steam turbine development as a route for reducing annular losses in the turbine stage endwall region. Active and passive clearance control for labyrinth seals, new sealing technologies such as brush seals and leaf seals etc, have all received considerable attention as methods for reducing leakage and leakage interaction losses, with some notable successes such as retractable packing on steam turbine shaft glands. More recently some workers have started to look at end-wall contouring in relation to reducing leakage interaction effects, by masking the endwall gaps between the fixed and rotating blades [37]. Figure 13 shows a number of modern impulse technology and 50% reaction technology steam turbine blade designs. All of these designs feature integral shrouding at the blade endwalls. Individual blades of this type are made by numerically controlled machining from solid bar material. The implications for manufacturing from introducing new endwall features are therefore relatively minor.

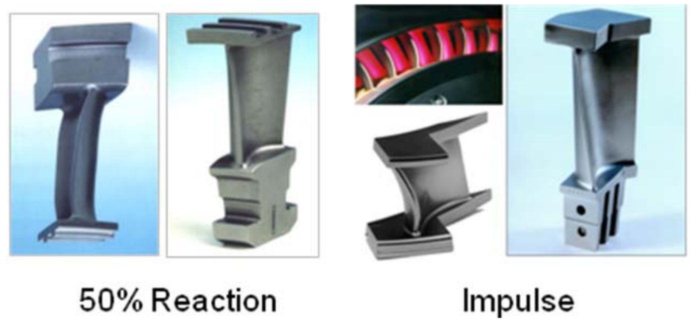


**FIGURE 13**. MODERN 3-D STEAM TURBINE BLADE DESIGNS FEATURING INTEGRAL SHROUDS (Courtesy of ALSTOM Power)

Endwall profiling of the type discussed in this paper could be readily implemented on steam turbine blade designs of the type shown in Figure 13, with minimal impact on production and manufacturing cost. Designs equivalent to those shown in this paper, could be implemented on the platforms of integral shroud steam turbine blades, without any need to stray outside of the original blade envelope. The impact on product cost for turbines that employ modern 3-D integral shrouded blade designs will therefore be small.

The potential therefore exists to further improve steam turbine short height blade designs by applying endwall profiling to the fixed and moving blade passages.

## CONCLUSIONS

1. A planar endwall CFD simulation has modelled the secondary flow features that exist within the blade passage with sufficient fidelity to base an optimisation system on.
2. A method has been deployed that parametrises the endwall for optimisation. The process of generating, meshing and running the CFD flow analysis has been automated.
3. A design system has been developed which utilises heuristic methods to seek the optimal endwall profile. The design methodology uses the principles of Darwin's selection of the fittest and the open nature of the system provides Engineers with an understanding of how certain geometric features influence the resulting flow field within a cascade blade row.
4. The source code for the design system is available for download at *www.dur.ac.uk/g.l.ingram* under an open source software license.
5. A profiled endwall design has been produced using the de-

sign system with an objective function based on secondary kinetic energy and compared to a design produced using an objective function based on an $U^3$ integral.
6. The $U^3$ integral is not an objective function that is suitable for endwall profile design without the ability to modify the two dimensional blade surface.
7. The merits and challenges of applying these profiled endwalls to the high pressure and intermediate pressure stages of steam turbines have been discussed and the potential for successful application seems high.


## ACKNOWLEDGMENT

The assistance of Dr Henk Slim from the High Speed Computing Service within Durham University is gratefully acknowledged.


## REFERENCES


[1] Harvey, N., Rose, M., Taylor, M., Shahpar, S., Hartland, J., and Gregory-Smith, D., 2000. "Nonaxisymmetric turbine end wall design: Part i a three-dimensional linear design system". *Journal of Turbomachinery,* ***122***(2), pp. 278–285.

[2] Hartland, J., Gregory-Smith, D., Harvey, N., and Rose, M., 2000. "Nonaxisymmetric turbine end wall design: Part ii experimental validation". *Journal of Turbomachinery,* ***122***(2), pp. 286–293.

[3] Praisner, T., Allen-Bradley, E., Grover, E., Knezevici, D., and Sjolander, S., 2007. "Application of non-axisymmetric endwall contouring to conventional and high-lift turbine airfoils.". *ASME Paper No. GT2007-25279*.

[4] Sieverding, C., 1985. "Recent progress in the understanding of basic aspects of secondary flows in turbine blades passages". *Transactions of the ASME, Journal of Engineering for Gas Turbines and Power,* ***107***, p. 248.

[5] Langston, L., 2001. "Secondary flows in axial turbines-a review". *Annals of the New York Academy of Sciences: Heat Transfer in Gas Turbine Systems*.

[6] Gregory-Smith, D., Graves, C., and Walsh, J., 1987. "Growth of secondary losses and vorticity in an axial turbine cascade.". *ASME Paper 87-GT-114*.

[7] Moustapha, S., Paron, G., and Wade, J., 1985. "Secondary flows in cascades of highly loaded turbine blades". *Transactions of the ASME, Journal of Engineering for Gas Turbines and Power,* ***107***, October, pp. 1031–1038.

[8] Langston, L., Nice, M., and Hooper, R., 1977. "Three-dimensional flow within a turbine cascade passage". *Transactions of the ASME, Journal of Engineering for Power,* ***99***, January, pp. 21–28.

[9] Eckerle, W., and Langston, L., 1987. "Horseshoe vortex formation around a cylinder". *Transaction of the ASME, Journal of Turbomachinery,* ***109***, April, pp. 278–285.

[10] Atkins, M., 1987. "Secondary losses and end-wall profiling in a turbine cascade.". *Proceedings of the Institution of Mechanical Engineers, International Conference, Turbomachinery: Efficiency Prediction and Improvement*(C255/87), September, pp. 29–42.

[11] Rose, M., 1994. "Non-axisymmetric endwall profiling in the hp ngv's of an axial flow gas turbine". *ASME Paper 94-GT-249*.

[12] Brennan, G., Harvey, N., Rose, M., Formison, N., and Taylor, M., 2001. "Improving the efficiency of the trent 500 hp turbine using non-axisymmetric end walls: Part 1 turbine design". *ASME Paper 2001-GT-0444*.

[13] Harvey, N., Brennan, G., Newman, D., and Rose, M., 2002. "Improving turbine efficiency using non-axisymmetric end walls: Validation in the multi-row environment and with low aspect ratio blading.". *ASME Paper GT-2002-30337*.

[14] Harrison, S., 1990. "The influence of blade lean on turbine losses.". *ASME 90-GT-55*.

[15] Sharma, O., Kopper, F., Stetson, G., Magge, S., Price, F., and Ni, R., 2003. "A perspective on the use of physical and numerical experiments in the advancement of design technology for axial flow turbines.". *XVI International Symposium on Air Breathing Engines (ISABE), Cleveland Ohio*.

[16] Bagshaw, D., Ingram, G., Gregory-Smith, D., and Stokes, M., 2005. "An experimental study of reverse compound lean in a linear turbine cascade.". *Proc. I.Mech.E. Series A: J. Power and Energy*.

[17] Sauer, H., Muller, R., and Vogeler, K., 2000. "Reduction of secondary flow losses in turbine cascades by leading edge modification at the endwall". *ASME Paper 2000-GT-0473*.

[18] Saha, A., Mahmood, G., and Acharya, S., 2006. "The role of leading-edge contouring on end-wall flow and heat transfer: Computations and experiments". *ASME Paper No. GT2006-90390*.

[19] Zess, G., and Thole, K., 2002. "Computational design and experimental evaluation of using a leading edge fillet on a gas turbine vane". *Transactions of the ASME, Journal of Turbomachinery*.

[20] Becz, S., Majewski, M., and Langston, L., 2004. "An experimental investigation of contoured leading edges for secondary flow loss reduction". *ASME Paper No. GT2004-53964*.

[21] Nagel, M. G., and Baier, R.-D., 2003. "Experimentally verified numerical optimisation of a 3d parameterised turbine vane with non-axisymmetric end walls". *ASME Paper GT2003-38624*.

[22] Bagshaw, D., Gregory-Smith, D., Ingram, G., Stokes, M., and Harvey, N., 2008. "The design of three dimensional turbine blades combined with profiled endwalls". *Proc. I.Mech.E. Series A: J. Power and Energy*.

[23] Bagshaw, D., Gregory-Smith, D., Ingram, G., and Stokes, M., 2008. "An experimental study of three dimensional

turbine blades combined with profiled endwalls". *Proc. I.Mech.E. Series A: J. Power and Energy*.

[24] Haller, B., and Anderton, J., 2002. "Development of new high load/high lift transonic shrouded hp gas turbine stage design - a new appraoch for turbomachinery". *ASME Paper GT-2002-30363*.

[25] MacPherson, R., 2009. "Endwall profile design for the durham cascade". Master's thesis, School of Engineering, Durham University.

[26] MacPherson, R., and Ingram, G., 2010. "Endwall profile design for the durham cascade using genetic algorithms". *Seventh South African Conference on Computational and Applied Mechanics,SACAM10 Pretoria,January 2010*.

[27] McIntosh, J. M., 2010. "Endwall profile design for the durham cascade". Master's thesis, School of Engineering and Computing Sciences, Durham University.

[28] Goldberg, D., 1989. *Genetic Algorithms in Search, Optimisation and Machine Leaning*. Addison-Wesley.

[29] Ingram, G., Gregory-Smith, D., and Harvey, N., 2005. "Investigation of a novel secondary flow feature in a turbine cascade with end wall profiling.". *Journal of Turbomachinery,* ***127***, pp. 209–214.

[30] Moore, H., and Gregory-Smith, D., 1996. "Transition effects on secondary flows in a turbine cascade". *ASME Paper 96-GT-100*.

[31] Haupt, R., and Haupt, S., 204. *Practical Genetic Algorithms with CD-ROM*. John Wiley & Sons, Inc.

[32] Michalewicz, Z., 1992. *Genetic Algorithms + Data Structures = Evolution Programs*. Springer-Verlag.

[33] Denton, J., 1993. "Loss mechanisms in turbomachines". *ASME Paper 93-GT-435*.

[34] Gregory-Smith, D., Ingram, G., Jayaraman, P., Harvey, N., and Rose, M., 2001. "Non-axisymmetric turbine end wall profiling". *Proceedings of the Institution of Mechanical Engineers,* ***215***(Part A), pp. 721–734.

[35] Ingram, G., 2003. "Endwall profiling for the reduction of secondary flow in turbines". PhD thesis, School of Engineering, University of Durham.

[36] Walker, P., and Hesketh, J., 1999. "Design of low reaction steam turbine blades". *Proc. I.Mech.E. Part C Journal of Mech. Eng. Sci,* ***213***(2), pp. 157–171.

[37] Hesketh, J., Hogg, S., and Stephen, D., 2003. "A stage efficiency prediction method and related performance aspects of retrofits on disc/diaphragm steam turbines". *ASME Int. Joint Power Generation Conference, Atlanta*(IJPGC-40145).